1-1-2008

Base-induced decomposition of alkyl hydroperoxides in the gas phase. Part 3. Kinetics and dynamics in HO + CH3OOH, C2H5OOH, and tert-C4H9OOH reactions

Shuji Kato
University of Colorado

G Barney Ellison
University of Colorado

Veronica Bierbaum
University of Colorado

Stephen J. Blanksby
University of Wollongong, blanksby@uow.edu.au

Base-induced decomposition of alkyl hydroperoxides in the gas phase. Part 3. Kinetics and dynamics in HO + CH3OOH, C2H5OOH, and tert-C4H9OOH reactions

Abstract

The $E_{CO}2$ elimination reactions of alkyl hydroperoxides proceed via abstraction of an α-hydrogen by a base: $X^- + R^1R^2HCOOH \rightarrow HX + R^1R^2CO + HO^-$. Efficiencies and product distributions for the reactions of the hydroxide anion with methyl, ethyl, and *tert*-butyl hydroperoxides are studied in the gas phase. On the basis of experiments using three isotopic analogues, $HO^- + CH_3OOH$, $HO^- + CD_3OOH$, and $H^{18}O^- + CH_3OOH$, the overall intrinsic reaction efficiency is determined to be 80% or greater. The $E_{CO}2$ decomposition is facile for these methylperoxide reactions, and predominates over competing proton transfer at the hydroperoxide moiety. The CH_3CH_2OOH reaction displays a similar $E_{CO}2$ reactivity, whereas proton transfer and the formation of HOO^- are the exclusive pathways observed for $(CH_3)_3COOH$, which has no α-hydrogen. All results are consistent with the $E_{CO}2$ mechanism, transition state structure, and reaction energy diagrams calculated using the hybrid density functional B3LYP approach. Isotope labeling for $HO^- + CH_3OOH$ also reveals some interaction between H_2O and HO^- within the $E_{CO}2$ product complex $[H_2O\cdots CH_2O\cdots HO^-]$. There is little evidence, however, for the formation of the most exothermic products $H_2O + CH_2(OH)O^-$, which would arise from nucleophilic condensation of CH_2O and HO^-. The results suggest that the product dynamics are not totally statistical but are rather direct after the $E_{CO}2$ transition state. The larger $HO^- + CH_3CH_2OOH$ system displays more statistical behavior during complex dissociation.

Keywords

Base, induced, decomposition, alkyl, hydroperoxides, gas, phase, Part, Kinetics, dynamics, CH3OOH, C2H5OOH, tert, C4H9OOH, reactions

Disciplines

Life Sciences | Physical Sciences and Mathematics | Social and Behavioral Sciences

Publication Details

Kato, S., Ellison, G., Bierbaum, V. & Blanksby, S. J. (2008). Base-induced decomposition of alkyl hydroperoxides in the gas phase. Part 3. Kinetics and dynamics in HO + CH3OOH, C2H5OOH, and tert-C4H9OOH reactions. The Journal of Physical Chemistry Part A: Molecules, Spectroscopy, Kinetics, Environment and General Theory, 112 (39), 9516-9525.

Base-Induced Decomposition of Alkyl Hydroperoxides in the Gas Phase. Part 3. Kinetics and Dynamics in the HO^- + CH_3OOH, C_2H_5OOH, and *tert*-C_4H_9OOH Reactions

Shuji Kato[1]*, G. Barney Ellison[1], Veronica M. Bierbaum[1], Stephen J. Blanksby[2]*

[1]Department of Chemistry and Biochemistry, University of Colorado and JILA, University of Colorado and National Institute of Standards and Technology, Boulder, CO 80309, U.S.A.

[2]School of Chemistry, University of Wollongong, NSW 2522, Australia

*Corresponding authors: Shuji.Kato@colorado.edu, blanksby@uow.edu.au

Abstract

The $E_{CO}2$ elimination reactions of alkyl hydroperoxides proceed via abstraction of an α-hydrogen by a base: $X^- + R^1R^2HCOOH \rightarrow HX + R^1R^2C{=}O + HO^-$. Efficiencies and product distributions for the reactions of the hydroxide anion with methyl, ethyl, and *tert*-butyl hydroperoxides are studied in the gas phase. Based on experiments using three isotopic analogues, $HO^- + CH_3OOH$, $HO^- + CD_3OOH$, and $H^{18}O^- + CH_3OOH$, the overall intrinsic reaction efficiency is determined to be 80% or greater. The $E_{CO}2$ decomposition is facile, for these methylperoxide reactions, and predominates over competing proton transfer at the hydroperoxide moiety. The CH_3CH_2OOH reaction displays a similar $E_{CO}2$ reactivity whereas proton transfer and formation of HOO^- are the exclusive pathways observed for $(CH_3)_3COOH$, which has no α-hydrogen. All results are consistent with the $E_{CO}2$ mechanism, transition state structure, and reaction energy diagrams calculated using the hybrid density functional B3LYP approach. Isotope labeling, for $HO^- + CH_3OOH$, also reveals some interaction between H_2O and HO^- within the $E_{CO}2$ product complex $[H_2O \cdots CH_2{=}O \cdots HO^-]$. There is little evidence, however, for the formation of the most exothermic products $H_2O + CH_2(OH)O^-$, which would arise from nucleophilic condensation of $CH_2{=}O$ and HO^-. The results suggest that the product dynamics are not totally statistical but are rather direct after the $E_{CO}2$ transition state. The larger $HO^- + CH_3CH_2OOH$ system displays more statistical behavior during complex dissociation.

Introduction

Base-induced $E_{CO}2$ elimination of alkyl peroxides $X^- + R^1R^2HCOOR^3 \rightarrow HX + R^1R^2C{=}O + R^3O^-$ is a variant of concerted E2 elimination reactions. The mechanism was proposed for solution reactions more than 50 years ago by Kornblum and DeLaMare;[1] the reaction initiates via an attack of a base anion (X^-) on an α-hydrogen[1,2] similar to the conventional E2 transformation. Unlike E2 reactions forming C=C double bonds, however, $E_{CO}2$ reactions produce stable carbonyl C=O bonds and can be quite exothermic. The $E_{CO}2$ reaction is considerably less explored in part because it is limited to peroxides (and a few other species such as methylnitrite[3] (CH_3ONO) and dimethyl methylphosphonate[4] [$(CH_3O)_2(CH_3)PO$] but it could have important implications.[5] For example, polyunsaturated fatty acid residues of phospholipids are extremely sensitive to oxidation during biochemical oxidative stress.[6-8] If lipid peroxides undergo $E_{CO}2$ reactions, they will be converted to highly genotoxic, unsaturated aldehydes and ketones[9,10] that are causative sources for cancer, aging, and pathology.[6,8,11] Despite the potential biochemical interest, the anionic $E_{CO}2$ mechanism of peroxide decomposition has been controversial in solution and in vivo because trace amounts of transition metal ions can afford an analogous product distribution via Fenton chemistry.[2,12]

Recently, a model reaction of $F^- + CH_3OOH \rightarrow HF + CH_2{=}O + HO^-$ has been studied in the gas phase[5] in which interferences due to adventitious metal ions or solvent molecules have been rigorously eliminated. The gas phase results are totally consistent with the proposed $E_{CO}2$ mechanism, and intriguing features are observed for the $E_{CO}2$ reactivity: The measured rate constant is about 50 % of the ion-molecule collision rate.[5] The calculated potential energy diagram indicates i) a transition state significantly below the reactant energy, ii) an extremely shallow potential well for the pre-reaction complex, and iii) a large amount of energy release after the $E_{CO}2$ transition state.[5] The rapidity of the reaction may well be rationalized in terms of the transition state energy that supports favorable kinetics. Furthermore, following the $E_{CO}2$ transformation, the hydroxide anion appears to leave the product complex [$HF \cdots CH_2O \cdots HO^-$]

without undergoing condensation with formaldehyde to form the most stable product pair HF + $CH_2(OH)O^-$.[5] The deep potential well minimum in the product potential energy surface seems to be avoided in analogy to the S_N2 reaction of $HO^- + CH_3F$.[13] Most recently, Hase and coworkers conducted a direct dynamics trajectory study of this reaction that supported the experimental observations.[14] The post-transition state dynamics do not follow the intrinsic reaction coordinate (IRC) path, which forms the $[CH_2(OH)_2 \cdots F^-]$ potential energy minimum on the IRC, with a 105 kcal mol^{-1} reaction exothermicity, and subsequently the dissociation products $CH_2(OH)O^-$ + HF with an energy release of 63 kcal mol^{-1}. Instead, formation of $HF + CH_2O + HO^-$ with an energy release of 27 kcal mol^{-1} is the major reaction channel.[14]

Intrinsic efficiencies of base-induced decomposition and the product dynamics, however, are yet to be fully characterized experimentally. For instance, it is unknown why the F^- + CH_3OOH rate constant is considerably below the collision limit, even though it is fairly rapid;[5] the energetics around the key transition state would suggest a significantly higher reaction efficiency. It was conjectured that the apparently smaller-than-unity efficiency of the F^- + CH_3OOH reaction may be due to HO^- abstracting a proton from HF within the dissociation complex, thereby regenerating the F^- reactant: in effect a novel anion-catalyzed decomposition reaction.[5] It then follows that another type of product dynamics involving an interaction between HO^- and HF may need to be considered. We have extended the study of base-induced decomposition of alkyl hydroperoxides to the reactions of superoxide[15] and reported direct observation of the Haber-Weiss reaction in the gas phase; the reaction has been controversial in solution over many decades. The superoxide reactions are also efficient, and produce another major product of ozonide presumably via a mechanism associated with the open-shell character of the reagent base anion.[15]

In the present paper we study the ion-molecule reaction of the hydroxide anion with methyl hydroperoxide to further characterize the base-induced chemical transformation that can now be observed in the isolation of the gas phase. The HO^- anion is more basic than F^- so that the reaction is expected to involve an exothermic proton transfer (PT) channel as well (Scheme

1). Competition between the PT and $E_{CO}2$ pathways is viewed as an internal prognosticator for the efficiency of the $E_{CO}2$ reaction. Theoretical calculations indicate that the rate-determining energetics, i.e., from the reactants to the pre-reaction complex to the $E_{CO}2$ transition state, are remarkably similar between the $F^- + CH_3OOH$ and $HO^- + CH_3OOH$ reactions. Following the $E_{CO}2$ transition state, the $HO^- + CH_3OOH$ system is significantly more downhill energetically than $F^- + CH_3OOH$ and non-statistical behavior may be persistent or even more pronounced.

Scheme 1

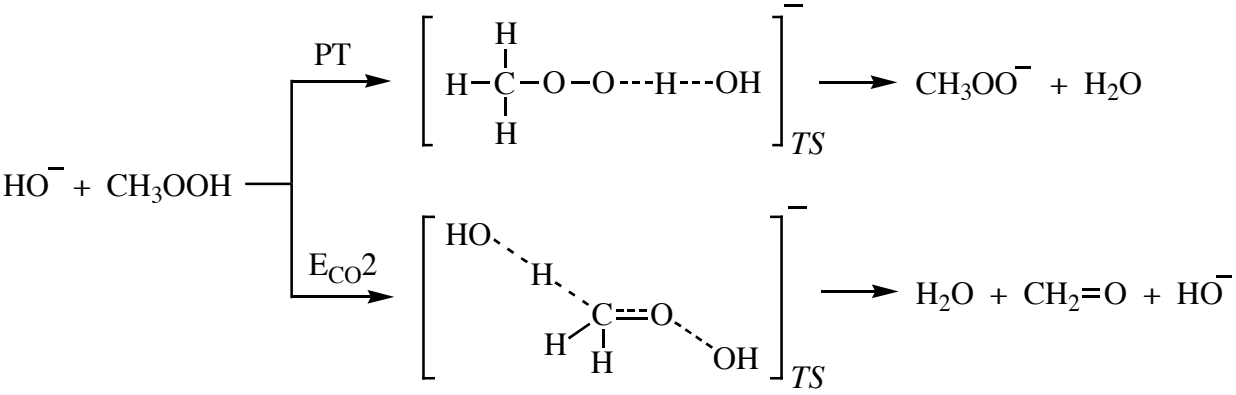

The $E_{CO}2$ pathway yields the same ionic product as the reactant anion. Isotope analogs are used to differentiate the reaction products and mechanism and to extract the intrinsic efficiency of the $E_{CO}2$ reaction (eqs 1 – 3). The site-specific isotope labeling also allows for quantitative elucidation of dynamical processes occurring within the product complex. The $E_{CO}2$ reaction is studied for a larger system of ethyl hydroperoxide (eq 4) and the effects of size and complexity on the dynamics are examined. The reaction of HO^- with *tert*-C_4H_9OOH (eq 5), which bears no α-hydrogen, is also studied for comparison and completeness.

$$HO^- + CH_3OOH \rightarrow H_2O + CH_2O + HO^- \quad (1)$$

$$HO^- + CD_3OOH \rightarrow HOD + CD_2O + HO^- \quad (2)$$

$$H^{18}O^- + CH_3OOH \rightarrow H^{18}OH + CH_2O + H^{16}O^- \quad (3)$$

$HO^- + CH_3CH_2OOH \rightarrow H_2O + CH_3CHO + HO^-$ (4)

$HO^- + (CH_3)_3COOH \rightarrow$ (no $E_{CO}2$ reaction) (5)

Experimental

All reactions in the present study used hydroxide anions HO^-, not DO^-, to elucidate the occurrence of $E_{CO}2$ mechanisms as well as the product dynamics after the key transition state. Reactions with DO^- could produce the same ionic product as derives from the $E_{CO}2$ scheme, via potential exchange at the peroxyl terminus, e.g., $DO^- + CH_3OOH \rightarrow [CH_3OO^- \cdots HOD] \rightarrow [CH_3OOD \cdots HO^-] \rightarrow CH_3OOD + HO^-$. Hydroxide anions were generated in the source section of the selected ion flow tube (SIFT) instrument,[16,17] mass selected, and injected into the reaction flow tube (0.5 Torr He), where the anions are collisionally thermalized to room temperature (≈ 300 K) before ion-molecule reactions initiate. Methyl and ethyl hydroperoxides were synthesized as described previously.[18] *tert*-Butyl hydroperoxide was purchased as a commercial sample (Aldrich) and used without further purification except for drying to remove water. Extreme care was taken in preparation, handling, and storage of these unstable and potentially explosive compounds. The neutral reagents were introduced into the reaction flow tube to react with HO^-, and ionic species were detected with the mass filter located at the downstream end of the flow tube.

Measurements were made after flowing the peroxide reagent for typically 20 minutes or longer in the stream of HO^- until the entire inlet system was adequately passivated and conditioned to reach a stationary state as monitored by the mass spectrometer. This was also important to evaporatively remove diethyl ether, a major synthetic impurity in methyl and ethyl hydroperoxides. In a separate experiment, the reaction of diethyl ether with HO^- produced comparable amounts of $C_2H_5O^-$ and $C_2H_5O^-(H_2O)$ at m/z 45 and m/z 63, respectively, essentially duplicating previous results.[19-22] A small amount of the signature product m/z 63 was indeed observed in the beginning of passivation with the synthetic alkyl hydroperoxides. The peroxide

reagent flows were maintained until the m/z 63 species largely disappeared.

Kinetics measurements with HO^- were performed by adding a constant flow of alkyl hydroperoxide via multiple inlets located along the reaction flow tube. Depletion of HO^- and formation of ionic products was monitored as a function of the inlet position which determines the reaction time. Mass discrimination effects were minimized across the mass range for the products but no further corrections were made. Although the reactions take place in a pseudo-first-order fashion with a large excess of the neutral reagents, complications arise in the kinetics of alkyl hydroperoxides with HO^-. For non-labeled hydroxide reactant, a major and characteristic $E_{CO}2$ product is the same hydroxide anion. Secondary reactions, which are in many cases $E_{CO}2$ reactions, also usually occur extensively for these reactive species. The reaction rate constants and branching ratios for primary products were thus determined from analysis of the kinetics using extrapolation to zero reaction time combined with a full coupled rate equation approach. Product yields (%) are presented as derived from the intrinsic primary branching. Reaction efficiency is defined as the ratio of the measured rate constant to the calculated collision rate constant. For the $H^{18}O^- + CH_3OOH$ reaction, the reactant anion $H^{18}O^-$ was mass-selected from HO^- at natural abundance in the source flow tube. Because of the low ion intensity, regular ion kinetics measurements were not performed. Instead, the reaction was examined back-to-back with the non-labeled $H^{16}O^- + CH_3OOH$ reaction. Given the same flow rate of the same neutral reagent, semi-logarithmic depletions of $\ln[H^{18}O^-]/[H^{18}O^-]_0$ and $\ln[H^{16}O^-]/[H^{16}O^-]_0$ were measured and the relative rate constant for $H^{18}O^-$ determined.

Stated error bars in rate constants represent one standard deviation of repeated measurements. The experimental rate constants also usually contain absolute uncertainties of ± 20% due to the overall measurement procedures.[16,17] The systematic errors, however, cancel in comparing the rate constants for different alkyl hydroperoxide reactions. Furthermore, examinations of several simple exothermic reactions in comparison with both literature values and calculated collision rate constants indicate that the absolute error bars are substantially smaller in this study. Systematic uncertainties due to sample purity cannot be entirely

eliminated, however. Despite all efforts to minimize impurities and in situ decomposition of the reagents, it is possible that the alkyl hydroperoxides are not 100% pure in the flow tube. Non-reactive impurities will slightly reduce the reaction efficiency. It should thus be noted that experimental reaction efficiencies may still be their lower limits.

Geometry optimizations were carried out with the B3LYP method[23,24] using the modest 6-31+G(d) basis set within the GAUSSIAN03 suite of programs.[25] All stationary points of the potential energy surfaces were characterized as either minima (no imaginary frequencies) or transition states (one imaginary frequency) by calculation of the frequencies using analytical gradient procedures. Frequency calculations provided zero-point energies, which were corrected by the empirical scaling factor of 0.9804 and added to the calculated electronic energy.[26] For the $HO^- + CH_3OOH$ potential (Figure 2) the minima connected by a given transition state were confirmed by intrinsic reaction coordinate calculations[27,28] while for the $HO^- + CH_3CH_2OOH$ potential (Figure 4) the connectivity was assigned by comparison of transition states with their methyl analogues and by inspection of the animated imaginary frequencies using the Gaussview or MOLDEN[29] packages. In some instances, single point energy calculations were conducted on each of the stationary point geometries using the CCSD(T) method[30] and the correlation consistent basis set aug-cc-pVDZ.[31] The electronic energies, zero-point energies, and geometries of important stationary points are provided as supporting information.

Collision rate constants were evaluated via the parametrized trajectory collision rate theory[32] using the polarizabilities[33] of 4.05, 5.85, and 9.50 x 10^{-24} cm^3 and electric dipole moments of 1.66, 1.77, and 1.84 D calculated at B3LYP/6-31+G(d)[25] for CH_3OOH, C_2H_5OOH, and *tert*-C_4H_9OOH, respectively.

Results

HO^- + CH_3OOH reaction

Figure 1 shows the kinetics decay of the hydroxide anion in the reaction of HO^- + CH_3OOH (eqs 6 and 7). CH_3OO^- is the major product (≈ 92%) formed from exothermic proton transfer ($\Delta_{rxn}H_{298} = -15.7$ kcal mol^{-1}).[18,34]

$$HO^- + CH_3OOH \rightarrow CH_3OO^- + H_2O \qquad 92\% \quad (6)$$

A small amount of methoxide anion (≈ 8%) is the other observed product. It was seen that all alkyl hydroperoxides in the present study formed minor amounts of corresponding alkoxide anions (6 – 8%). The formation mechanism is unknown (see below), and the alkoxide channels will not be explicitly shown in the equations and schemes.

A strong deviation from linearity is observed in the later stage of the semi-logarithmic kinetics plot (Figure 1). Two features are clearly seen. First, the initial decay of HO^- is unusually slow for this highly exothermic proton transfer system. The rate constant is determined from the initial slope to be $k = 7.6 \pm 0.2 \times 10^{-10}$ cm^3 s^{-1}, accounting for only 29% of the calculated collision rate (2.64×10^{-9} cm^3 s^{-1}). This strongly suggests the occurrence of a competing $E_{CO}2$ pathway (eq 7), which invisibly reproduces HO^-.

$$HO^- + CH_3OOH \rightarrow H_2O + CH_2O + HO^- \qquad (7)$$

Secondly, the decay of HO^- eventually stops as the CH_3OO^- signal reaches a plateau at about a 50% height (Figure 1), establishing a stationary state between the two anions. This is caused by the facile secondary reaction of CH_3OO^- that regenerates the HO^- reactant via an $E_{CO}2$ mechanism (eqs 8 and 9).

$$CH_3OO^- + CH_3OOH \rightarrow [CH_3OOH \cdots CH_2O \cdots HO^-] \rightarrow HO^- (+ \text{neutrals}) \quad (8)$$

$$\rightarrow [H_2O \cdots CH_2O \cdots HO^- \cdots CH_2O] \rightarrow HO^- (+ \text{neutrals}) \quad (9)$$

Methyl peroxide anion ($\Delta_{acid}H_{298}(CH_3OOH)$ = 374.6 kcal mol^{-1}) is even more basic than F^- ($\Delta_{acid}H_{298}(HF)$ = 371.3 kcal mol^{-1}) and is expected to be $E_{CO}2$ active. Because of the chemical reactivity, formation of a simple adduct $CH_3OO^-(CH_3OOH)$ is very minor as observed experimentally.

HO^- + CD_3OOH reaction

The kinetics plot for the decay of HO^- with CD_3OOH is also displayed in Figure 1. While similar deviation from linearity is observed, the decay of HO^- is faster with CD_3OOH than with CH_3OOH. The rate constant is determined from the initial slope to be k = 10.2 ± 0.2 x 10^{-10} cm^3 s^{-1} (efficiency 39% with respect to the collision rate). In addition to the proton-transfer product CD_3OO^- (≈ 80%), DO^- is observed among the products. DO^- is formed presumably via intracomplex H/D exchange following the initial $E_{CO}2$ transformation (eqs 11 and 12).[5]

$$HO^- + CD_3OOH \rightarrow CD_3OO^- + H_2O \quad 80\% \quad (10)$$

$$HO^- + CD_3OOH \rightarrow [HOD \cdots CD_2O \cdots HO^-] \rightarrow HO^- + CD_2O + HOD \quad (11)$$

$$\rightarrow [DO^- \cdots CD_2O \cdots H_2O] \rightarrow DO^- + CD_2O + H_2O \quad 13\% \quad (12)$$

In the later stage of the kinetics, the HO^- signal reaches a lower plateau than that observed in the HO^- + CH_3OOH reaction (Figure 1), while the proton-transfer product CD_3OO^- has a plateau at about the same height of 50%. Formation of the additional DO^- product mostly accounts for the faster decay of the parent ion. The results suggest that the faster reaction of HO^- + CD_3OOH is facilitated primarily by the formation of the additional visible product through post-transition state H/D exchange, and not by a difference in the rate kinetics at the $E_{CO}2$ barrier (or by a possible difference in the reagent purities between CH_3OOH and CD_3OOH). Primary deuterium

kinetic isotope effects would instead favor $E_{CO}2$ elimination of CH_3OOH over that of CD_3OOH. As will be discussed later, the intrinsic kinetic isotope effects are likely very small for these systems.

The HO^- + CD_3OOH reaction also produced a trace amount (< 1%) of species at m/z 46, which is assigned to deuterated formate DCO_2^-.[35] The formate anion is an intrinsic product from the reaction and not due to deprotonation of formic acid DCOOH, a possible contaminant. Our experiment on the HO^- + HCOOH reaction yielded two anionic products HCO_2^- and $HO^-(H_2O)$ with the ratio of ~ 3 : 1, as similarly reported by Tanner et al.[36] The DCO_2^- anion was observed from the HO^- + CD_3OOH reaction whereas HO^-(HDO), the signature species for DCOOH, was missing.

$H^{18}O^-$ + CH_3OOH reaction

The rate of loss for $H^{18}O^-$ is 2.4 ± 0.1 times faster than the rate of loss for HO^- in the reaction with CH_3OOH, as measured in the linear regime of the kinetics (Figure 1). This result gives the rate constant of k = 18.0 ± 0.9 x 10^{-10} cm^3 s^{-1}, considerably closer to the collision rate (efficiency 71%). Approximately 40% of $H^{16}O^-$ is formed with respect to the parent ion loss (eq 14), consistent with the $E_{CO}2$ reaction scheme in which the anion abstracts an α hydrogen on the methyl group with concerted elimination of the terminal hydroxide anion as the product.

$$H^{18}O^- + CH_3OOH \rightarrow CH_3OO^- + H^{18}OH \quad (13)$$

$$H^{18}O^- + CH_3OOH \rightarrow [H^{18}OH \cdots CH_2O \cdots H^{16}O^-] \rightarrow H^{16}O^- + CH_2O + H^{18}OH \quad (14)$$

$$\rightarrow [H^{18}O^- \cdots CH_2O \cdots H^{16}OH] \rightarrow H^{18}O^- + CH_2O + H^{16}OH \quad (15)$$

By analogy to the HO^- + CD_3OOH reaction, intracomplex proton exchange must be occurring to regenerate the $H^{18}O^-$ reactant (eq 15).

HO^- + CH_3CH_2OOH reaction

The measured rate constant is k = 12.9 ± 0.2 x 10^{-10} cm^3 s^{-1} with an efficiency of 45%. Proton transfer (eq 16) is a major reaction observed. The $E_{CO}2$ reaction (eq 17) is invisible, but intracomplex rearrangement can yield deprotonated acetaldehyde (eq 18), the other major product observed. A minor amount of HOO^- is attributed to a competing elimination reaction with abstraction of a β hydrogen from C_2H_5OOH (eq 19). Nucleophilic substitution at the α carbon could also conceivably produce HOO^- (see Table 1) but is excluded based on the absence of this product channel in the HO^- + CH_3OOH system. The overall reaction is relatively slow despite the exothermic proton transfer ($\Delta_{rxn}H_{298}$ = −19.3 kcal mol^{-1}). This result is explained by the invisible $E_{CO}2$ channel to regenerate HO^- thereby apparently slowing down the overall kinetic decay of HO^-.

$HO^- + CH_3CH_2OOH \rightarrow CH_3CH_2OO^- + H_2O$ 35% (16)

$HO^- + CH_3CH_2OOH \rightarrow [H_2O \cdots CH_3CHO \cdots HO^-] \rightarrow HO^- + CH_3CHO + H_2O$ (17)

$\rightarrow [H_2O \cdots CH_2CHO^- \cdots H_2O] \rightarrow CH_2CHO^- + 2H_2O$ 53% (18)

$HO^- + CH_3CH_2OOH \rightarrow HOO^- + CH_2CH_2 + H_2O$ 5% (19)

HO^- + $(CH_3)_3COOH$ reaction

The measured rate constant is k = 21.0 ± 1.0 x 10^{-10} cm^3 s^{-1} (efficiency 69%). Proton transfer (eq 20) is a major reaction observed. The other major product HOO^- is assigned to a competing elimination reaction (eq 21).[37] The overall reaction still appears to be slow considering the large exothermicity for proton transfer ($\Delta_{rxn}H_{298}$ = −20.1 kcal mol^{-1}).

$HO^- + (CH_3)_3COOH \rightarrow (CH_3)_3COO^- + H_2O$ 47% (20)

$HO^- + (CH_3)_3COOH \rightarrow HOO^- + (CH_3)_2CCH_2 + H_2O$ 44% (21)

Kinetic analysis for methyl hydroperoxides

Reaction schemes for the hydroxide anions can be constructed from the measured rate constants and product distributions (Schemes 2 – 4). In these schemes, the branching fractions are displayed as the reaction rate for channel *i* normalized to the collision rate (k_i / k_{col}). In the HO^- + CH_3OOH reaction, direct proton transfer accounts for 27% of collisions (Scheme 2) while an additional 2% is for methoxide formation (not shown). 71% of collisions result in no apparent loss of HO^-; this result is the sum of the invisible $E_{CO}2$ pathway (α) and non-reactive collisions ($1 - \alpha$).

Scheme 2

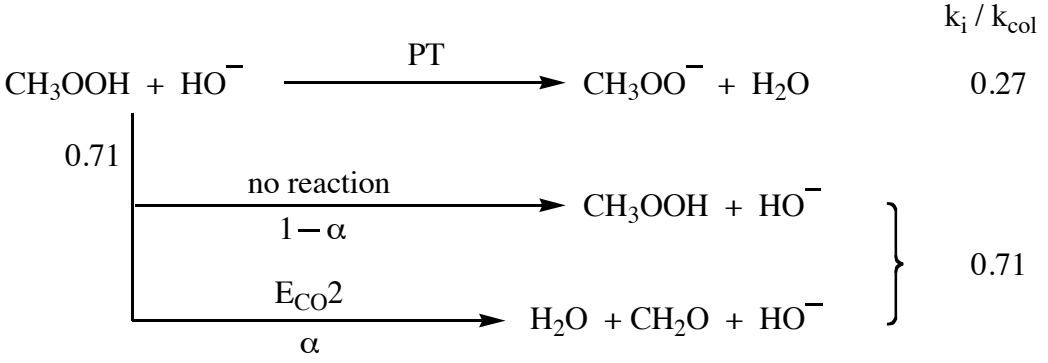

In the HO^- + CD_3OOH reaction (Scheme 3), invisible pathways to give HO^- are to account for 61% of total collisions based on the measured reaction efficiency. With the H/D scrambling scheme, a fraction (β) of HO^- converts to DO^- within the $E_{CO}2$ product complex (observed DO^- branching fraction ≅ 5% of collisions). The $[DO^-]/[HO^-]$ ratio thus must be $\alpha\beta/(1 - \alpha\beta) = 0.05/0.61 \cong 0.08$. Since α is separately determined to be 0.75 from the $H^{18}O^-$ reaction (see below), the isotope-scrambling probability β is obtained as 0.10. Regeneration of HO^- via the $E_{CO}2$ channel then accounts for $0.66 \times \alpha(1 - \beta) = 0.45$, thus giving the probability for non-reactive collision as 16%. Intrinsic reaction efficiencies (including $E_{CO}2$ regeneration of HO^-) are determined to be 84% and 50% for the overall reaction and $E_{CO}2$ channel, respectively.

Scheme 3

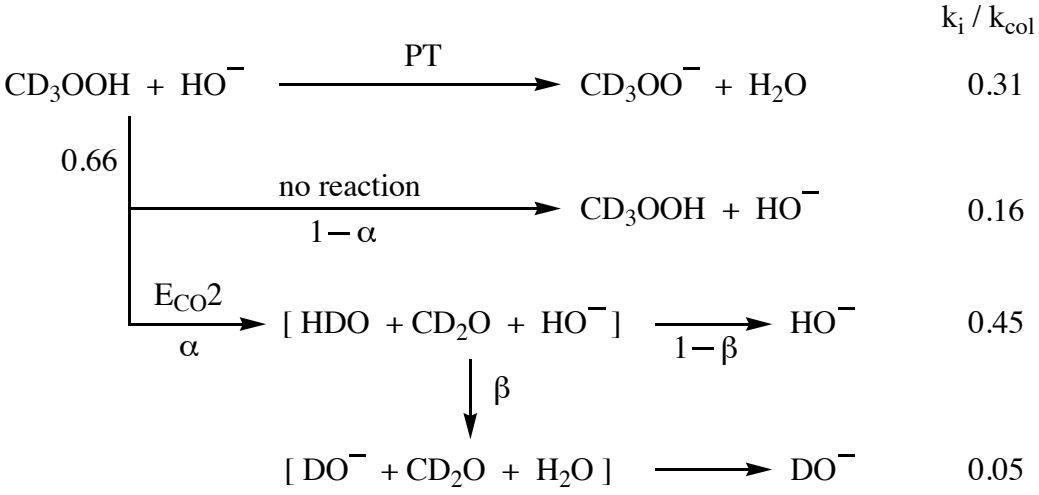

It is reasonable to assume that the $H^{18}O^-$ + CH_3OOH reaction (Scheme 4) produces the same amount of proton-transfer product CH_3OO^- (27%) as the non-labeled HO^- + CH_3OOH reaction. It is also a good approximation from the reaction degeneracy that the isotope-scrambling probability to form $H^{18}O^-$ (γ) is two times greater than that forming DO^-; the very large exothermicity for the $E_{CO}2$ pathway ($\Delta_{rxn}H_{298}$ = −54.6 kcal mol^{-1}) would diminish isotope effects (kinetic/equilibrium) in the hydroxide-water exchange. From the experimental DO^- branching fraction of about 5% (Scheme 3), the branching fraction for $E_{CO}2$ regeneration of $H^{18}O^-$ must thus be 11%. This requires that $\alpha\gamma = 0.15$ (Scheme 4). Production of $H^{16}O^-$ from the $H^{18}O^-$ reactant is the origin of the faster reaction of $H^{18}O^-$ + CH_3OOH as compared to $H^{16}O^-$ + CH_3OOH which regenerates $H^{16}O^-$. The observed efficiency ratio is 2.5 between these reactions. This places an additional requirement that $\alpha(1 - \gamma) = 0.60$. $\alpha = 0.75$ and $\gamma = 0.20$ are finally obtained. The branching fractions for $H^{16}O^-$ formation and non-reactive collision are then calculated to be 42% and 18%, respectively (Scheme 4).[38] Intrinsic efficiencies (including $E_{CO}2$ regeneration of $H^{18}O^-$) are determined to be 82% and 53% for the overall reaction and $E_{CO}2$ channel, respectively.

Scheme 4

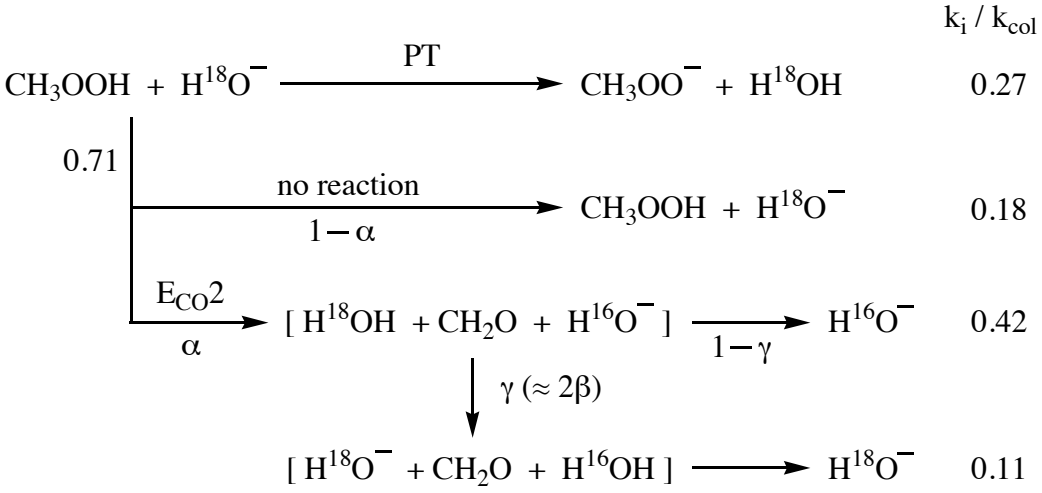

Discussion

Reaction mechanisms

Table 1 lists reaction enthalpies for HO^- reacting with CH_3OOH, C_2H_5OOH, and *tert*-C_4H_9OOH. Relative energies on the [HO^-, CH_3OOH] potential energy surface are shown in Figure 2 at the B3LYP/6-31+G(d) and CCSD(T)/aug-cc-pVDZ//B3LYP/6-31+G(d) levels of theory. The CCSD(T) computations reproduce experimental heats of reaction particularly well (Table 1) and the computationally cheaper B3LYP calculations agree well with the CCSD(T) results with the exception of product energies involving formaldehyde, suggesting that the hybrid density functional approach should be suitable for larger systems. The computations account for the overall features of the observed reactions. The $E_{CO}2$ reaction proceeds via the characteristic transition state (TS1), an anti-periplanar structure that is consistent with the synchronous E2 reaction mechanism (Figure 3). The proton transfer reaction is energetically allowed and highly exothermic. No reaction was observed from CH_3OO^- + H_2O, also consistent with the computations that the reactant energy is lower than both TS1 and the preceding transition state TS2 for rearrangement of the HO^- species.

At the B3LYP level of theory, the HO^- + C_2H_5OOH reaction (Figure 4) has proton

transfer and $E_{CO}2$ energetics that are very similar to $HO^- + CH_3OOH$. Proton transfer and $E_{CO}2$ reaction enthalpies agree fairly well with experimental values (Table 1). Formation of the $^-CH_2CHO$ anion via intracomplex proton transfer (eq 18) is a highly exothermic process ($\Delta_{rxn}H_{298}$(experimental) = −83.6 kcal mol^{-1}) and is a major product channel observed experimentally. The $E_{CO}2$ channel is not available for $(CH_3)_3COOH$ because it has no α-hydrogen; the absence of $E_{CO}2$ reactivity has been demonstrated in the similar reaction of F^- + $(CH_3)_3COOH$.[5]

Both the C_2H_5OOH and *tert*-C_4H_9OOH reactions show the additional product HOO^- that is absent from the CH_3OOH system. This strongly suggests the involvement of β-hydrogens in the reaction. Instead of concerted E2 elimination, a slightly different E1cb mechanism has been identified computationally for $HO^- + C_2H_5OOH$ (eqs 22 and 23).

$$HO^- + CH_3CH_2OOH \rightarrow [H_2O \cdots {}^-CH_2CH_2OOH]_{E1cb} \quad (22)$$

$$\rightarrow [H_2O \cdots CH_2CH_2 \cdots {}^-OOH] \rightarrow HOO^- + CH_2CH_2 + H_2O \quad (23)$$

Here, deprotonated $^-CH_2CH_2OOH$ is a stable structure within the ion-molecule complex as the carbanion is stabilized by the water molecule and intramolecular interaction with the -OOH moiety (Figure 5). Following further rearrangement via TS5 (Figure 4) the E1cb reaction yields the same products as the conventional E2 mechanism. It is interesting to note that in the HO^- + CH_3OOH reaction an analogous $^-CH_2OOH$ structure is not stable but connects directly to the TS1 transition state. Formation of HOO^- from HO^- + *tert*-C_4H_9OOH may be via either E2 or E1cb, subtly dependent on the stability of the $^-CH_2(CH_3)_2COOH$ structure. Notably, overall the elimination pathways are somewhat endothermic both experimentally and computationally for the C_2H_5OOH and *tert*-C_4H_9OOH reactions (Table 1). Formation of HOO^- can be explained as follows. In the TS5 transition state, H_2O and HOO^- are sterically separated by the intervening ethylene species. TS5 could thus dissociate to a product pair of $[HOO^- \cdots CH_2CH_2]$ and H_2O,

with the calculated exothermicity of 2.4 kcal mol^{-1} (Figure 4). The [$HOO^- \cdots CH_2CH_2$] product is only weakly bound by 7.8 kcal mol^{-1} so that it will subsequently dissociate to HOO^- and CH_2CH_2; we have observed that ion clusters with binding energies of 15 kcal mol^{-1} or smaller generally do not survive the high-pressure flow tube at room temperature. Alternatively, the B3LYP calculations predict that the reaction is exoergic ($\Delta_{rxn}G_{298} = -5.7$ kcal mol^{-1}) although it is endothermic ($\Delta_{rxn}H_{298} = +6.4$ kcal mol^{-1}) so that the entropy may play a role in promoting these irreversible transformations.

Nucleophilic substitution (S_N2) reactions are energetically accessible for all the alkyl hydroperoxides (Table 1). S_N2 reactions at α-carbons are similarly and moderately exothermic ($\Delta_{rxn}H_{298} \approx -5$ kcal mol^{-1}) eliminating HOO^-. The $S_N2(\alpha)$ reaction, however, does not seem to be competitive with other facile reaction channels; HOO^- was not observed from $CH_3OOH + HO^-$, which has the least steric hindrance and lowest kinetic barrier [39] towards the S_N2 transformation $HO^- + CH_3OOH \rightarrow [HOCH_3 \cdots {}^-OOH]$. Sequential intracomplex proton transfer to yield CH_3O^- + HOOH is even less exothermic (−0.1 kcal mol^{-1}) and improbable. Given the fact that $S_N2(\alpha)$ transformation is even less likely to occur for ethyl and *tert*-butyl hydroperoxides, production of $C_2H_5O^-$ + HOOH and *tert*-$C_4H_9O^-$ + HOOH cannot take place even though they are slightly more exothermic ($\Delta_{rxn}H_{298} = -3.4$ and −7.7 kcal mol^{-1}, respectively). The $S_N2(\alpha)$ mechanism was investigated computationally for the $HO^- + CH_3CH_2OOH$ potential and the barrier to the reaction (via TS7 in Figure 4) was found to be 5.0 kcal mol^{-1} above the entrance channel. Thus on the basis of experimental and computational observations the $S_N2(\alpha)$ mechanism is unlikely and does not account for the observed formation of HOO^- or alkoxide anions.[40,41] S_N2 reactions at β-carbons (e.g., $HO^- + CH_3CH_2OOH \rightarrow [HOCH_3 \cdots {}^-CH_2OOH] \rightarrow CH_3OH + CH_2O + HO^-$) are highly exothermic in ethyl and *tert*-butyl reactions (Table 1). The barrier to this process, however, is very high and the $S_N2(\beta)$ mechanism should be excluded; the associated transition state for the ethyl reaction (TS8, Supporting Information) is 74.3 kcal mol^{-1} higher in energy relative to the reactants.

We computationally identify yet another pathway for $HO^- + C_2H_5OOH$ that yields

ethylene oxide and regenerates hydroxide via TS6 (Figure 4). Along the reaction energy diagram all intermediates and transition states are below the reactants. IRC analysis indicates that TS6 does connect the [$H_2O \cdots HOO^- \cdots CH_2CH_2$] complex with the epoxide complex. A similar mechanism with *tert*-C_4H_9OOH would form 2,2-dimethyl oxirane *cyc*-$CH_2C(CH_3)_2O$. In CID of $C_2H_5OO^-$ and *tert*-$C_4H_9OO^-$ anions, analogous formation of epoxides is a plausible and significant mechanism for the observed production of HO^- at relatively high collision energies.[42] If the epoxide pathway is occurring substantially in the HO^- + C_2H_5OOH and *tert*-C_4H_9OOH reactions, it provides an additional mechanism to account for the apparent slowness of the overall reactions below the collision rates.

Intrinsic $E_{CO}2$ efficiencies

The isotope labeling revealed the overall efficiency for the HO^- + CH_3OOH reaction to be 80% or greater (recall that the efficiency is the lower limit if non-reactive impurities are present in the neutral reagent; see Experimental.) The $E_{CO}2$ decomposition is the major process (efficiency ≈ 50% of collision) whereas proton transfer is less effective (≈ 30% of collision). For comparison, in the F^- + CH_3OOH reaction,[5] the $E_{CO}2$ reactivity represents most of the overall efficiency (49%) while proton transfer is slightly endothermic and only an upper bound is given for the efficiency (< 5%). The HO^- + CH_3OOH reaction is a rare example in which a competing chemical pathway predominates over an exothermic, barrierless proton transfer that would otherwise proceed at unit efficiency.[43] Associative detachment may similarly compete with proton transfer in the reaction of *o*-benzyne with HO^-.[44,45] From the other perspective, the $E_{CO}2$ reactivity could even approach unit efficiency if proton transfer were not competing. The high efficiency may be understood in terms of the energetics around the TS1 transition state, which is 14.7 kcal mol^{-1} lower in energy than the reactants at the CCSD(T) level of theory and follows an extremely shallow pre-reaction complex well (−14.8 kcal mol^{-1}). The energetics compare well with those for F^- + CH_3OOH; the pre-reactive complex and the transition state are 15.9 and 14.6 kcal mol^{-1} lower in energy than the reactants, respectively, at the same level of theory.[5] Once the

pre-reaction complex is formed from CH_3OOH and HO^- (or F^-), access to the TS1 transition state should be facile. Such unusually shallow wells for the pre-reaction complexes (0.1 and 1.3 kcal mol^{-1} relative to the transition states for HO^- and F^-, respectively) suggest that their lifetimes may be sufficiently short so that intramolecular vibrational energy redistribution is incomplete and, thus, their unimolecular kinetics are non-RRKM.[46,47] Addressing this intriguing question is beyond the scope of the experimental and computational approach in this study.

The calculated bond lengths indicate subtle but important differences between the HO^- + CH_3OOH and F^- + CH_3OOH reactions. The TS1 for HO^- + CH_3OOH is even closer to the reactants (free CH_3OOH) than is the TS1 for F^- + CH_3OOH (Table 2).[48,49] At the transition state, the C−H and O−O bonds are elongated by only about 0.1 Å (as compared to ≈ 0.2 Å for F^-) while the C−O bond is shortened by only about 0.04 Å (≈ 0.08 Å for F^-). The TS1 for HO^- + CH_3OOH is thus characterized by a very early transition state, qualitatively consistent with the significantly larger reaction exothermicity (54.6 kcal mol^{-1}, in comparison to 35.6 kcal mol^{-1} for F^- + CH_3OOH). A similar conclusion can be drawn for HO^- + CH_3CH_2OOH (Table 2). The *intrinsic* primary deuterium kinetic isotope effect (KIE) for $E_{CO}2$ transformations of HO^- + CH_3OOH versus HO^- + CD_3OOH is thus expected to be very small, while it can still be normal ($k_H/k_D > 1$) typical of concerted E2 reactions. In addition, the overall reaction efficiencies including proton transfer are sufficiently large that they approach saturation. These factors should combine to make the overall KIE very close to unity for ensembles immediately after the TS1 transition states. While moderately rapid E2 reactions of diethyl ether display KIE values of 2 – 7 in the gas phase at ambient temperature,[20,22,50] the KIE values are essentially unity for rapid E2 reactions of *tert*-butyl halides.[51] The argument justifies the assignment that the observed faster reaction of HO^- + CD_3OOH (and hence the apparently inverse KIE) reflects, in reality, the post-transition state H/D exchange.

$E_{CO}2$ product dynamics

The DO^- product observed from the HO^- + CD_3OOH reaction strongly suggests H/D

scrambling that involves HOD and HO^- in the complex prior to dissociation (eqs 11 and 12). The kinetic analysis shows the ratio of HO^- to DO^- from this complex to be roughly 9 : 1 (Scheme 3). The experimental results suggest encounters of hydroxide and water species during the complex lifetime, although the scrambling is incomplete far below the statistical partitioning limit of $[HO^-] : [DO^-] = 2 : 1$. A similar H/D scrambling involving hydrogen fluoride and hydroxide anion has been suggested from observation of DO^- in the $E_{CO}2$ reaction of F^- + CD_3OOH,[5] that is, $[DF \cdots CD_2O \cdots HO^-] \Leftrightarrow [HF \cdots CD_2O \cdots DO^-]$ yielding HO^- and DO^- with a ratio of ~ 16 : 1.[52] In the fluoride case, a larger fraction of hydrogen fluoride – hydroxide anion encounters would lead to regeneration of F^- via exothermic proton transfer. This process could contribute to the apparent reduction in reaction efficiency to below unity although it is difficult to quantify this effect experimentally.

Direct dynamics trajectory calculations,[14] however, predict that such an intracomplex interaction between HF and HO^- is negligible. Instead, approximately 30% of the F^- + CH_3OOH encounters (55 out of 200 trajectories) result in direct back-dissociation to the reactants,[14] providing another very feasible explanation for the less-than-unity reaction efficiency. Although TS1 has an energy approximately 15 kcal mol^{-1} below that of the reactants for both F^- + CH_3OOH and HO^- + CH_3OOH at CCSD(T)/aug-cc-pVDZ//B3LYP/6-31+G(d), it is possible that a collision with a large impact parameter and orbital angular momentum results in a large rotational energy at TS1. If there is poor coupling between the orbital motion and the internal degrees of freedom for the complex, the effective potential energy increases at TS1 and reduction of the $E_{CO}2$ reaction efficiency may result. This mechanism has been discussed to explain the less-than-unity efficiency in the S_N2 reaction of F^- + CH_3Cl,[53,54] for which the transition state energy is about 12 kcal mol^{-1} below the reactants.

Intriguingly, there is little indication that the leaving hydroxide anion and formaldehyde interact within the product complex. Consider the labeled reaction.

$$HO^- + CD_3OOH \rightarrow [HOD \cdots CD_2O \cdots HO^-]$$

$$\rightarrow [HOD \cdots CD_2(OH)O^-]^* \rightarrow CD_2(OH)O^- \quad (24)$$

$$\rightarrow [HOD \cdots DCO_2^- \cdots HD]^* \rightarrow DCO_2^- \quad (25)$$

The deprotonated diol anion $CD_2(OH)O^-$ can form from nucleophilic condensation of hydroxide and formaldehyde (eq 24), and its formation is very exothermic (Figure 3). Termolecular association between hydroxide and formaldehyde has been measured to be very rapid forming the diol anion.[36] Nonetheless, the expected $CD_2(OH)O^-$ anion (m/z 49) was not observed from $HO^- + CD_3OOH$, nor previously from the $F^- + CD_3OOH$ reaction.[5] The diol anion could alternatively lose dihydrogen within the complex to yield the formate anion (eq 25), a major species observed in metastable and collision-induced decompositions of CH_3OO^- via the intermediacy of the diol species.[55] Based on the structure, energy, and intrinsic reaction coordinate (IRC) calculations at the B3LYP/6-311++G** level of theory,[55] an isolated $CD_2(OH)O^-$ anion will 1,2-eliminate HD to yield DCO_2^- with the barrier height and reaction enthalpy of about 26 and –23 kcal mol^{-1}, respectively.[55] The DCO_2^- anion was observed but with only a very minor yield (< 1%) from the reaction of HO^- with CD_3OOH. Reexamination of the $F^- + CD_3OOH$ results[5] also reveals negligible formation of DCO_2^- (< 0.5%).

Back-dissociation of $[HOD \cdots CD_2(OH)O^-]^* \rightarrow [HOD \cdots CD_2O \cdots HO^-]$ may be the only other possibility for the fate of the deprotonated diol, if it is ever formed within the complex. Isolated $CH_2(OH)O^-$ can dissociate to CH_2O and HO^- with no exit barrier ($\Delta_{rxn}H_{298} \approx$ 32 kcal mol^{-1}), in good competition with the H_2 elimination channel which has the lower but tight activation barrier.[55] In fact, in both the metastable and high-energy collision-induced dissociations of CH_3OO^-, the deprotonated diol intermediate yields comparable amounts of HO^- and HCO_2^-.[55] This suggests that formation and back-dissociation of the diol anion is a minor process when the HCO_2^- yield is also small. There are caveats to this proposition, however. In the low-energy collision-induced dissociation of CH_3OO^-, the hydroxide anion was the major

product whereas formation of the formate was extremely minor.[42]

In view of the varying results on diol decomposition, which are both interesting and puzzling, it is unlikely that the methyl hydroperoxide results can be discussed based solely on the energetics when the product dynamics display non-statistical behavior. Theoretical studies will greatly aid in revealing these processes. For the $E_{CO}2$ channel of the $F^- + CH_3OOH$ reaction, the direct dynamics calculations[14] indicate that the hydroxide anion directly leaves the $[HF \cdots CH_2O \cdots HO^-]$ complex while avoiding the deep potential well minimum to form the diol complex, which is the IRC product following TS1. Since the $HO^- + CH_3OOH$ system has a very similar potential energy feature up to TS1 and is even more steeply downhill energetically after TS1 towards the products, it is very likely that the product dynamics are also direct.

The larger $C_2H_5OOH + HO^-$ system displays more statistical behavior, i.e., a substantial interaction between HO^- and CH_3CHO within the product complex to produce the acetaldehyde enolate anion (eq 18). The potential energy diagram (Figure 4) indicates that formation of deprotonated diol $CH_3CH(OH)O^-$ is even more exothermic. There is no experimental evidence, however, for the intermediacy of the $[M - H]^-$ diol anion. The observed $[M - H]^-$ product exhibits reactivity essentially due to the $C_2H_5OO^-$ anion from proton transfer.[56] Energetically,[42] the diol anion could also lose dihydrogen to yield the acetate anion (m/z 59). No such species was observed from the $C_2H_5OOH + HO^-$ reaction within detection limits. The exothermic irreversible transformation within the complex, i.e., from acetaldehyde (eq 17) to the enolate anion (eq 18), obviously predominates over the diol anion formation. In any case, for the ethyl reaction, the nascent HO^- interacts strongly with the carbonyl within the product complex. The differential behaviors of HO^- strongly suggest that the product dynamics switch from direct to more statistical in going from the methyl to ethyl hydroperoxides, potentially reflecting different degrees of intramolecular vibrational redistribution (IVR) during complex dissociation.[46] Effects of size and complexity on the dynamics are being systematically studied for a variety of peroxides and base anions.

Conclusions

Reactions of HO^- with several alkyl hydroperoxides were studied in the gas phase to shed light on the $E_{CO}2$ reactivity and dynamics of potential biochemical importance. The intrinsic efficiency for the reaction of methyl hydroperoxide with HO^- is determined to be > 80% (overall) and > 50% ($E_{CO}2$ channel), with the $E_{CO}2$ reaction predominating over the exothermic proton transfer channel. The $E_{CO}2$ reactivity could approach unit efficiency if the competing proton transfer channel were not available. Ethyl hydroperoxide reacts with HO^- via $E_{CO}2$ and proton transfer pathways plus an additional E1cb channel. *tert*-Butyl hydroperoxide has a reactivity similar to ethyl hydroperoxide except for the lack of the $E_{CO}2$ channel. Calculated potential energy diagrams are very similar around the key $E_{CO}2$ transition states for the reactions of HO^- + CH_3OOH and HO^- + C_2H_5OOH as well as for F^- + CH_3OOH, consistent with the high $E_{CO}2$ efficiencies observed. The $E_{CO}2$ transition state for HO^- + CH_3OOH is even closer to the reactants than is the transition state for F^- + CH_3OOH to the reactants. As expected, the primary deuterium kinetic isotope effect is very small for HO^- reacting with CH_3OOH versus CD_3OOH.

Following the $E_{CO}2$ transition state, the potential energy curves show steep descent towards the products. Little evidence is found for the formation of a deprotonated diol intermediate within the product complex [$H_2O \cdots CH_2O \cdots HO^-$], suggesting that the nascent hydroxide species leaves the complex with a negligible interaction with formaldehyde. The deep potential energy minimum for diol anion formation appears to be avoided, a non-IRC dynamics analogous to those predicted theoretically for the S_N2 reaction[13] of HO^- + CH_3F and $E_{CO}2$ reaction[14] of F^- + CH_3OOH. Besides the negligible diol anion formation, a proton-exchange interaction is suggested between the hydroxide and water species within the complex. The larger ethyl hydroperoxide system displays more statistical behavior so that the hydroxide anion interacts strongly with acetaldehyde in the product complex [$H_2O \cdots CH_3CHO \cdots HO^-$], forming $^-CH_2CHO$ as a major product. In addition to experiments and energetics discussions, direct

dynamics trajectory studies will be very helpful and insightful to probe the dynamical aspects of these $E_{CO}2$ reactions.

Acknowledgments

SK and VMB were supported by the National Science Foundation (CHE-0647088), SJB by the Australian Research Council (DP0452849), and GBE by the United States Department of Energy (DE-FG02-87ER13695) and the National Science Foundation (CHE-9813659). SJB also acknowledges the Australian Partnership for Advanced Computing (ANU, Canberra) for a generous allocation of supercomputer time. The authors thank Professor William L. Hase for helpful discussions as well as providing unpublished data. Supplementary experiments on diethyl ether and formic acid by Ms. Nicole Eyet are also appreciated.

Supporting Information Available: Geometries, electronic energies, zero-point energies, and imaginary frequencies used for Figures 2 and 4. This information is available free of charge via the Internet at http://pubs.acs.org.

References

(1) Kornblum, N.; DeLaMare, H. E. *J. Am. Chem. Soc.* **1951**, *73*, 880.
(2) Hiatt, R. In *Organic Peroxides*; Swern, D., Ed.; Wiley-Interscience: New York, 1971; Vol. 2, p. 1 and references therein.
(3) King, G. K.; Maricq, M.; Bierbaum, V. M.; DePuy, C. H. *J. Am. Chem. Soc.* **1981**, *103*, 7133.
(4) Lum, R. C.; Grabowski, J. J. *J. Am. Chem. Soc.* **1993**, *115*, 7823.
(5) Blanksby, S. J.; Ellison, G. B.; Bierbaum, V. M.; Kato, S. *J. Am. Chem. Soc.* **2002**, *124*, 3196.
(6) Halliwell, B.; Gutteridge, J. M. C. *Free Radicals in Biology and Medicine*, 3rd ed.; Oxford University Press: Oxford, 1999.
(7) Murphy, R. C.; Fiedler, J.; Hevko, J. *Chem. Rev.* **2001**, *101*, 479.
(8) Niki, E. Peroxides in Biological Systems. In *Organic Peroxides*; Ando, W., Ed.; John Wiley & Sons: New York, 1992.
(9) Burcham, P. C. *Mutagenesis* **1998**, *13*, 287.
(10) Marnett, L. J. *Carcinogenesis* **2000**, *21*, 361.

(11) Sies, H. *Oxidative Stress*; Academic Press: London, 1985.
(12) Hofmann, R.; Hübner, H.; Just, G.; Krätzsch, L.; Litkowez, A. K.; Pritzkow, W.; Rolle, W.; Wahren, M. *J. Prakt. Chem.* **1968**, *37*, 102.
(13) Sun, L.; Song, K.; Hase, W. L. *Science* **2002**, *296*, 875.
(14) López, J. G.; Vayner, G.; Lourderaj, U.; Addepalli, S. V.; Kato, S.; deJong, W. A.; Windus, T. L.; Hase, W. L. *J. Am. Chem. Soc.* **2007**, *129*, 9976.
(15) Blanksby, S. J.; Bierbaum, V. M.; Ellison, G. B.; Kato, S. *Angew. Chem. Int. Ed.* **2007**, *46*, 4948.
(16) Van Doren, J. M.; Barlow, S. E.; DePuy, C. H.; Bierbaum, V. M. *Int. J. Mass Spectrom. Ion Processes* **1987**, *81*, 85.
(17) Bierbaum, V. M. Flow Tubes. In *Encyclopedia of Mass Spectrometry, Vol 1, Theory and Ion Chemistry*; Gross, M. L., Caprioli, R., Eds.; Elsevier: Amsterdam, 2003; pp 276.
(18) Blanksby, S. J.; Ramond, T. M.; Davico, G. E.; Nimlos, M. R.; Kato, S.; Bierbaum, V. M.; Lineberger, W. C.; Ellison, G. B.; Okumura, M. *J. Am. Chem. Soc.* **2001**, *123*, 9585.
(19) DePuy, C. H.; Bierbaum, V. M. *J. Am. Chem. Soc.* **1981**, *103*, 5034.
(20) de Koning, L. J.; Nibbering, N. M. M. *J. Am. Chem. Soc.* **1987**, *109*, 1715.
(21) Spanel, P.; Pavlik, M.; Smith, D. *Int. J. Mass Spectrom. Ion Processes* **1995**, *145*, 177.
(22) Baschky, M. C.; Kass, S. R. *Int. J. Mass Spectrom.* **2000**, *195/196*, 411.
(23) Becke, A. D. *J. Chem. Phys.* **1993**, *98*, 5648.
(24) Lee, C.; Yang, W.; Parr, R. G. *Phys. Rev. B* **1988**, *37*, 785.
(25) Frisch, M. J.; Trucks, G. W.; Schlegel, H. B.; Scuseria, G. E.; Robb, M. A.; Cheeseman, J. R.; Montgomery, J. A., Jr.; Vreven, T.; Kudin, K. N.; Burant, J. C.; Millam, J. M.; Iyengar, S. S.; Tomasi, J.; Barone, V.; Mennucci, B.; Cossi, M.; Scalmani, G.; Rega, N.; Petersson, G. A.; Nakatsuji, H.; Hada, M.; Ehara, M.; Toyota, K.; Fukuda, R.; Hasegawa, J.; Ishida, M.; Nakajima, T.; Honda, Y.; Kitao, O.; Nakai, H.; Klene, M.; Li, X.; Knox, J. E.; Hratchian, H. P.; Cross, J. B.; Adamo, C.; Jaramillo, J.; Gomperts, R.; Stratmann, R. E.; Yazyev, O.; Austin, A. J.; Cammi, R.; Pomelli, C.; Ochterski, J. W.; Ayala, P. Y.; Morokuma, K.; Voth, G. A.; Salvador, P.; Dannenberg, J. J.; Zakrzewski, V. G.; Dapprich, S.; Daniels, A. D.; Strain, M. C.; Farkas, O.; Malick, D. K.; Rabuck, A. D.; Raghavachari, K.; Foresman, J. B.; Ortiz, J. V.; Cui, Q.; Baboul, A. G.; Clifford, S.; Cioslowski, J.; Stefanov, B. B.; Liu, G.; Liashenko, A.; Piskorz, P.; Komaromi, I.; Martin, R. L.; Fox, D. J.; Keith, T.; Al-Laham, M. A.; Peng, C. Y.; Nanayakkara, A.; Challacombe, M.; Gill, P. M. W.; Johnson, B.; Chen, W.; Wong, M. W.; Gonzalez, C.; Pople, J. A. *Gaussian 03, Revision B.05*; Gaussian, Inc.: Pittsburgh, PA, 2003.
(26) Scott, A. P.; Radom, L. *J. Phys. Chem.* **1996**, *100*, 16502.
(27) Gonzalez, C.; Schlegel, H. B. *J. Chem. Phys.* **1989**, *90*, 2154.
(28) Gonzalez, C.; Schlegel, H. B. *J. Phys. Chem.* **1990**, *94*, 5523.
(29) Schaftenaar, G.; Noordik, J. H. *J. Comput.-Aided Mol. Design* **2000**, *14*, 123.
(30) Bartlett, R. J. *J. Phys. Chem.* **1989**, *93*, 1697.
(31) Dunning Jr, T. H. *J. Chem. Phys.* **1989**, *90*, 1007.
(32) Su, T.; Chesnavich, W. J. *J. Chem. Phys.* **1982**, *76*, 5183.
(33) Miller, K. J.; Savchik, J. A. *J. Am. Chem. Soc.* **1979**, *101*, 7206.
(34) Unless otherwise specified, all thermochemical values are derived from P. J. Linstrom and W. G. Mallard, Eds., **NIST Chemistry WebBook, NIST Standard Reference Database Number 69**, June 2005, National Institute of Standards and Technology, Gaithersburg MD, 20899 (http://webbook.nist.gov).

(35) Identity of the corresponding HCO_2^- species is ambiguous from the CH_3OOH reaction because of the mass overlap with the residual $C_2H_5O^-$ anion.
(36) Tanner, S. D.; Mackay, G. I.; Bohme, D. K. *Can. J. Chem.* **1981**, *59*, 1615.
(37) A minor amount of deprotonated acetone (m/z 57) is also observed (≈ 1%). The origin is unknown however; it may arise from an acetone impurity either in the reagent or formed during the gas handling.
(38) Scheme 4 predicts the ratio of [formed $H^{16}O^-$]/[depleted $H^{18}O^-$] to be 0.60. The observed value of 0.40 (with error bars of ± 0.02 accounting only for the ion counting statistics) is somewhat smaller, but not unreasonable if one takes into account a systematic bias due to overall mass discrimination against $H^{16}O^-$ relative to $H^{18}O^-$ under experimental conditions. Small amounts of unknown reactive impurities such as diethylether would also contribute to $H^{18}O^-$ depletion without production of $H^{16}O^-$.
(39) DePuy, C. H.; Gronert, S.; Mullin, A.; Bierbaum, V. M. *J. Am. Chem. Soc.* **1990**, *112*, 8650.
(40) In search of a mechanism for alkoxide production, we attempted to locate transition states for S_N2 reactions at oxygen with no success so far. Alternatively, the alkoxide anions may possibly be formed from HO^- deprotonation of ROH impurities, which could be formed in situ under experimental conditions via heterogeneous decompositions of the alkyl hydroperoxides in the gas transfer line and/or the flow tube, as observed for HOOH (Ref. 41).
(41) Ramond, T. M.; Blanksby, S. J.; Kato, S.; Bierbaum, V. M.; Davico, G. E.; Schwartz, R. L.; Lineberger, W. C.; Ellison, G. B. *J. Phys. Chem. A* **2002**, *106*, 9641.
(42) Blanksby, S. J.; Kato, S.; Bierbaum, V. M.; Ellison, G. B. *Aust. J. Chem.* **2003**, *56*, 459.
(43) Ikezoe, Y.; Matsuoka, S.; Takebe, M.; Viggiano, A. *Gas Phase Ion-Molecule Reaction Rate Constants Through 1986*; Maruzen: Tokyo, 1987.
(44) Zhang, X.; Bierbaum, V. M.; Ellison, G. B.; Kato, S. *J. Chem. Phys.* **2004**, *120*, 3531.
(45) Zhang, X.; Kato, S.; Bierbaum, V. M.; Nimlos, M. R.; Ellison, G. B. *J. Phys. Chem. A.* **2004**, *108*, 9733.
(46) Baer, T.; Hase, W. L. *Unimolecular Reaction Dynamics*; Oxford University Press: New York, 1996.
(47) Robinson, P. J.; Holbrook, K. A. *Unimolecular Reactions*; Wiley: New York, 1972.
(48) Tyblewski, M.; Meyer, R.; Bauder, A. *8th Colloquium on High Resolution Molecular Spectroscopy*, Tours, France, 1983, cited in Haas et al. (Ref. 49).
(49) Haas, B.; Oberhammer, H. *J. Am. Chem. Soc.* **1984**, *106*, 6146.
(50) Bierbaum, V. M.; Filley, J.; DePuy, C. H.; Jarrold, M. F.; Bowers, M. T. *J. Am. Chem. Soc.* **1985**, *107*, 2818.
(51) Eyet, N.; Villano, S. M.; Kato, S.; Bierbaum, V. M. *J. Am. Soc. Mass Spectrom.* **2007**, *18*, 1046.
(52) In the earlier work, the ratio of HO^- to DO^- was reported to be ~ 6 : 1 (Ref. 5). The revised ratio comes from full analysis to extract the primary branching ratio, which corresponds to the relative product yields of HO^- (82%) and DO^- (5%).
(53) Su, T.; Wang, H.; Hase, W. L. *J. Phys. Chem. A* **1998**, *102*, 9819.
(54) Wang, H.; Hase, W. L. *J. Am. Chem. Soc.* **1997**, *119*, 3093.
(55) Schalley, C. A.; Schröder, D.; Schwarz, H.; Möbus, K.; Boche, G. *Chem. Ber.* **1997**, *130*, 1085.

Table 1. Reaction products and enthalpies for CH_3OOH, C_2H_5OOH, and *tert*-C_4H_9OOH.

reactants	reaction	products	reaction enthalpy[a]	
$CH_3OOH + HO^-$	PT	$CH_3OO^- + H_2O$	–15.7	(–17.8)[b]
	$E_{CO}2$	$HO^- + CH_2O + H_2O$	–54.6	(–55.6)[b]
	S_N2 (α)	$HOO^- + CH_3OH$	–5.6	
$CH_3CH_2OOH + HO^-$	PT	$CH_3CH_2OO^- + H_2O$	–19.3	(–19.6)[c]
	$E_{CO}2$	$HO^- + CH_3CHO + H_2O$	–59.1	(–55.3)[c]
	S_N2 (α)	$HOO^- + CH_3CH_2OH$	–5.2	(–8.5)[c]
	S_N2 (β)	$HO^- + CH_2O + CH_3OH$	–36.2	(–36.8)[c]
	E1cb	$HOO^- + C_2H_4 + H_2O$	5.7	(5.4)[c]
	epoxidation	$HO^- + cyc\text{-}CH_2CH_2O + H_2O$	–30.9	(–26.2)[c]
$(CH_3)_3COOH + HO^-$	PT	$(CH_3)_3COO^- + H_2O$	–20.1	
	S_N2 (α)	$HOO^- + (CH_3)_3COH$	–5.9	
	S_N2 (β)	$HO^- + (CH_3)_2CO + CH_3OH$	–42.9	
	E2/E1cb	$HOO^- + (CH_3)_2C{=}CH_2 + H_2O$	6.7	
	epoxidation	$HO^- + cyc\text{-}CH_2C(CH_3)_2O + H_2O$	not available	

[a] All experimental energies in kcal mol^{-1} at 298 K.[34]

[b] Calculated at CCSD(T)/aug-cc-pVDZ//B3LYP/6-31+G(d) with zero-point energy corrections (scaling factor 0.9804).

[c] Calculated at B3LYP/6-31+G(d) with zero-point energy corrections (scaling factor 0.9804).

Table 2. Bond lengths (Å) for $E_{CO}2$ transformations of CH_3OOH and CH_3CH_2OOH [a]

structure	O8–H7 [b]	H7–C4	C4–O3	O3–O2
$CH_3OOH + HO^-$ reaction				
CH_3OOH	____	1.095	1.419	1.461
			1.437[c]	1.443[c]
$[HO^- \cdots CH_3OOH]$	1.689	1.159	1.407	1.476
TS1 ($HO^- + CH_3OOH$)	1.561	1.200	1.384	1.577
$CH_3OOH + F^-$ reaction				
$[F^- \cdots CH_3OOH]$	1.647[b]	1.142	1.417	1.495
TS1 ($F^- + CH_3OOH$)	1.272[b]	1.303	1.341	1.686
$CH_3CH_2OOH + HO^-$ reaction				
CH_3CH_2OOH	____	1.097	1.429	1.460
$[HO^- \cdots CH_3CH_2OOH]$	1.696	1.157	1.408	1.533
TS1 ($HO^- + CH_3CH_2OOH$)	1.623	1.179	1.393	1.568

[a] Calculated at B3LYP/6-31+G(d). The numbering of the nuclei is shown in Figure 3. In all structures, the attacking anion is attached to an α-hydrogen (H7).

[b] F8–H7 lengths for $CH_3OOH + F^-$.

[c] Experimental.[48,49]

Figure captions:

Figure 1 Kinetic decays of hydroxide anions in the reactions of HO^- + CH_3OOH (open circle), HO^- + CD_3OOH (triangle), and $H^{18}O^-$ + CH_3OOH (square). The CH_3OO^- product from the HO^- + CH_3OOH reaction (closed circle) is also shown. The reaction times have been normalized to account for the different concentrations of methyl hydroperoxide reactants used in these experiments. The dash-dot line indicates the predicted decay of HO^- at the collision rate k_{col}.

Figure 2 Relative energies (kcal mol^{-1}) on the [HO^-, CH_3OOH] potential energy surface (electronic energy + zero-point energy) calculated at CCSD(T)/aug-cc-pVDZ//B3LYP/6-31+G(d). B3LYP/6-31+G(d) energies are also indicated in parentheses. All energies include a scaled (0.9804) zero-point energy correction.

Figure 3 Structure of the $E_{CO}2$ transition state (TS1) for the HO^- + CH_3OOH reaction calculated at the B3LYP/6-31+G(d) level of theory.

Figure 4 Relative energies (kcal mol^{-1}) on the [HO^-, CH_3CH_2OOH] potential energy surface (electronic energy + zero-point energy) calculated at B3LYP/6-31+G(d). All energies include a scaled (0.9804) zero-point energy correction.

Figure 5 Structure of the E_{1cb} stationary state for the HO^- + CH_3CH_2OH reaction calculated at the B3LYP/6-31+G(d) level of theory.

Figure 1

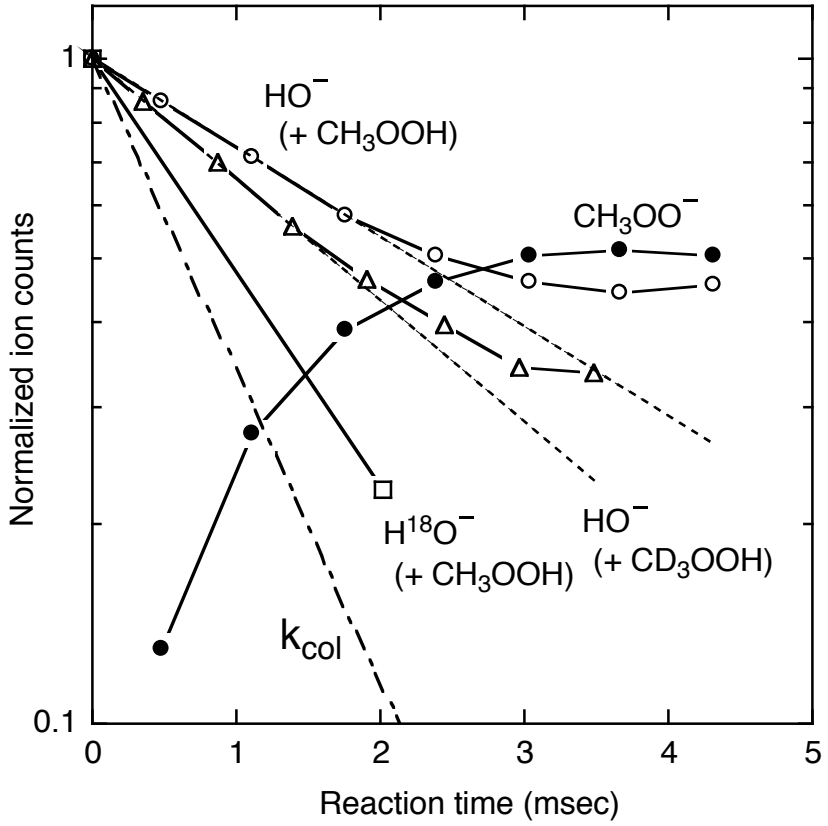
1
0.1
Normalized ion counts
0
1
2
3
4
5
Reaction time (msec)
HO⁻
(+ CH3OOH)
CH3OO⁻
H18O⁻
(+ CH3OOH)
HO⁻
(+ CD3OOH)
kcol

Figure 2

Figure 3

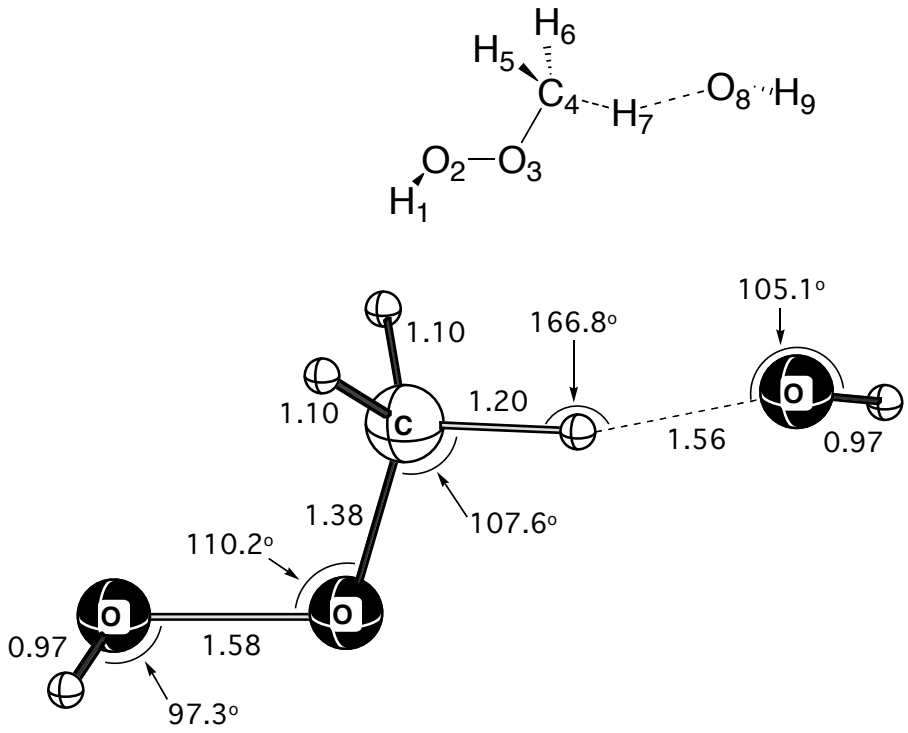
H6
H5
C4
H7
O8
H9
O2—O3
H1
105.1°
166.8°
1.10
1.10
C
1.20
1.56
O
0.97
1.38
107.6°
110.2°
O
O
0.97
1.58
97.3°

Figure 4

Figure 5

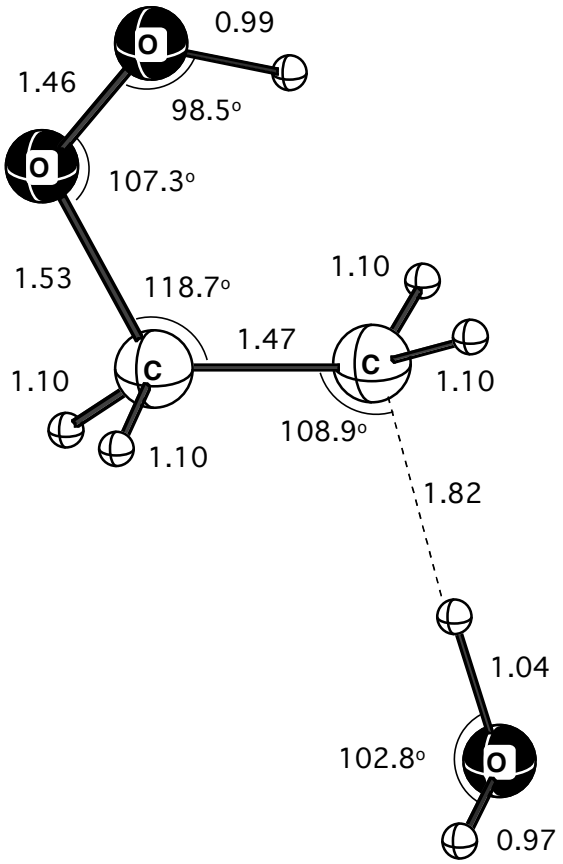
O
0.99
1.46
98.5°
O
107.3°
1.53
118.7°
1.10
1.47
C
C
1.10
1.10
108.9°
1.10
1.82
1.04
102.8°
O
0.97